Accepted Manuscript

Structure of a diffuse suture between Fennoscandia and Sarmatia in SE Poland based on interpretation of regional reflection seismic profiles supported by unsupervised clustering

Miłosz Mężyk, Michał Malinowski, and Stanisław Mazur

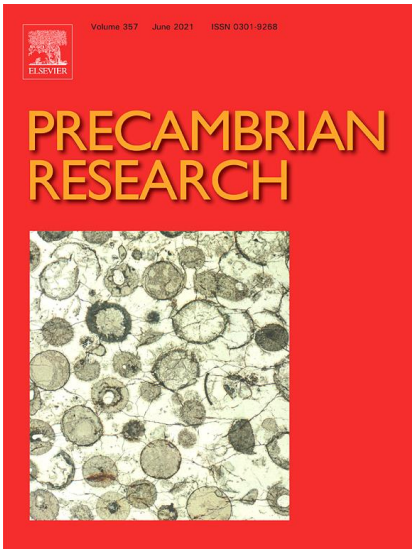

DOI:	10.1016/j.precamres.2021.106176
Reference:	PRECAM_106176
Appeared in:	Precambrian Research
Received date:	Jul 07, 2020
Revised date:	Jan 25, 2021
Accepted date:	Mar 08, 2021
Published date:	Mar 31, 2021

Please cite this article as:

Mężyk, M., Malinowski, M., Mazur, S., 2021. Structure of a diffuse suture between Fennoscandia and Sarmatia in SE Poland based on interpretation of regional reflection seismic profiles supported by unsupervised clustering. Precambrian Research 358. doi: 10.1016/j.precamres.2021.106176

Structure of a diffuse suture between Fennoscandia and Sarmatia in SE Poland based on interpretation of regional reflection seismic profiles supported by unsupervised clustering

Miłosz Mężyk[1], Michał Malinowski[1*], and Stanisław Mazur[2]

[1]Institute of Geophysics Polish Academy of Sciences, Warsaw, 01-452, Poland

[2]Institute of Geological Sciences Polish Academy of Sciences, 00-818, Warsaw, Poland

*Now at Geological Survey of Finland, P.O. Box 96, FI-02151, Espoo

Correspondence to: Milosz Mezyk (mmezyk@igf.edu.pl)

Abstract

The Paleoproterozoic suture between Sarmatia and Fennoscandia (SFS), two major components of the East European Craton, extends SW-ward from Russia through Belarus to SE Poland. The exact character of this suture remains speculative, despite the results of the wide-angle reflection and refraction (WARR) soundings. Here, we show results of newly reprocessed deep reflection seismic data of the PolandSPAN™ survey, portraying the whole crust and uppermost mantle in SE Poland. Their interpretation is supported by the unsupervised clustering of seismic reflectivity patterns. From the integration of PolandSPAN™ data with both magnetic and WARR data, we conclude that the SFS cannot be interpreted as a localised lithospheric discontinuity coincident with the Minsk Fault. Instead, we observe a so-called diffuse cryptic suture zone, c. 150 km wide, where materials from two colliding plates are mixed over large distances to form a unified continental crust. The suture-related reflections are interpreted as a thrust-wedge rooted at the lower-middle crust interface underneath the Ivanowo-Borisov zone. We support Bogdanova et al. (2015) view that the Okołowo-Holeszów Belt

and Belarus-Podlasie Granulite Belt have affinities to the NW margin of Sarmatia. We interpret both units as belonging to the diffuse SFS.

***Keywords**: East European Craton, Sarmatia, Fennoscandia, Suture, Precambrian, Paleoproterozoic, Collision, Seismic reflection, Crustal structure*

1. Introduction

Paleoproterozoic collision of Fennoscandia with Sarmatian and Volgo-Uralian crustal segments formed the East European Craton (EEC) (Bogdanova et al. 2008). After the amalgamation, the EEC has never undergone the complete disassembly, but its size and shape have changed during several successive extension-compression cycles along its margins (Bogdanova et al., 2005a; Gee and Stephenson, 2006). The Precambrian crystalline basement of the EEC is covered with a thick sequence of late Proterozoic and Phanerozoic sedimentary strata that deepens towards the Teisseyre-Tornquist Zone (TTZ) (Młynarski, 1982; Grad and Polkowski, 2016; Mikołajczak et al., 2019) exceeding the reach of densely-spaced deep research wells in this area (Krzemińska et al., 2017). This fact makes the geophysical methods crucial for drawing inferences about the crustal structure. The newly compiled total intensity magnetic anomaly map for the whole Poland (Petecki and Rosowiecka, 2017) depicts many short-wavelength anomaly variations in the EEC area that correlate well with tectonic units and magmatic intrusions in the Precambrian basement. The gravity anomaly map (Bielik et al., 2006) presents this province in a less heterogeneous way consisting of several gravity domains within which Bouguer anomalies tend to decrease at the EEC margin (e.g. Pomeranian Low, Podlasie Low, Lublin Low) or increase where a high crustal density of mafic rocks or metamorphic belts are present (e.g. the Mazury-Mazovia High and the Podlasie High, respectively). The crustal configuration of the SW margin of the EEC was also extensively explored using wide-angle reflection/ refraction (WARR) soundings (Grad et al., 2006a; Janik et al., 2009; Guterch et al., 2010), portraying relatively simple, three-layer, cratonic crust.

In 2012, the marginal part of the EEC in Poland was covered by an unprecedented network of ten PolandSPAN™ deep reflection seismic profiles (with a total length of 2200 km) that advanced our understanding of the sedimentary history, tectonic architecture, and basement structure of the lower Palaeozoic shale basins (Krzywiec et al., 2013). Seismic interpretation of these profiles served as constraints for potential field modelling that led to a new interpretation of the TTZ (Mazur et al., 2015, 2016a) and Polish Caledonides (Mazur et al., 2016b). Moreover, PolandSPAN™ data allowed to redefine the extent of Variscan deformation (Krzywiec et al., 2017a, b; Mazur et al., 2020) and prove that crystalline basement in SE Poland underwent substantial extension in the Neoproterozoic

(Krzywiec et al., 2018). Malinowski (2016) proved that the PolandSPAN™ data can be reprocessed to cover the whole crust. Mężyk et al. (2019) reprocessed several profiles from NE Poland to image the deeper crust and the crust-mantle boundary by applying the extended correlation method (Okaya and Jarchow, 1989). The strong mid- to lower crustal reflectivity along these reprocessed PolandSPAN™ profiles was interpreted as kilometre-scale S–C' shear zones invoking ductile extension of a hot orogenic crust during Svekofennian orogeny (Mężyk et al., 2019). The similar lower crustal reflectivity patterns were also detected along regional deep-seismic profiles acquired at this area, such as the POLCRUST-01 (Malinowski et al., 2013, 2015) and the reappraised profile VIII across the Pripyat Trough (Juhlin et al., 1996) or reported by the BABEL Working Group (1993) and FIRE deep-seismic program (Kukkonen and Lahtinen, 2006) in the Baltic Sea and Finland, respectively.

Here, we apply extended correlation processing to a subset of the PolandSPAN™ data located in SE Poland that are oriented perpendicular to the TTZ (dip profiles: 5000, 5100, 5200) and parallel to the TTZ (strike profiles: 1000, 1100) with a total length of ~ 1000 km. These new seismic reflection data complement our earlier research on the Fennoscandian-affinity crust in NE Poland. Altogether they allow for a better description of the long series of tectonic processes that led to the formation of the mid- to lower crust in the marginal part of the EEC, which turns out to be not so homogenous as commonly assumed based on deep refraction data. The key questions we would like to see resolved are as follows: (i) is a tectonic suture between the Fennoscandian and Sarmatian segments recognizable in the crustal reflectivity patterns? (ii) does the purported suture represent a localised zone that separates two continental terrains with a dissimilar pre-collisional structure or rather embrace an array of intercontinental high-strain zones? We start with the geological background and proceed further with a brief explanation of the processing steps including a novel clustering-based seismic attribute meant for enhancing deeper reflectivity and facilitating the interpretation process. Finally, we present the new results and integrate them with the existing geological observations to provide preliminary interpretation addressing the above key questions regarding the crustal structure of the EEC margin across the junction between Sarmatia and Fennoscandia.

Our concepts build upon earlier work by Svetlana Bogdanova, whose research has greatly contributed over the past decades to a better understanding of the structure and evolution of the EEC. Several

international collaborations (e.g., Bogdanova et al. 2008, 2015, 2016), including EUROBRIDGE deep seismic sounding project (Bogdanova et al., 2001, 2006), laid foundations to resolve the deep crustal architecture of the craton. We further develop the recent concepts by Bogdanova et al. (2015, 2016) regarding the location of a cryptic tectonic suture between Sarmatia and Fennoscandia and confirm a diffuse nature of this tectonic boundary that is probably situated farther north than previously believed.

2. Tectonic Setting and Crustal Structure

The most widely adopted tectonic model for the crustal evolution of the EEC is a three-unit configuration suggested by Bogdanova (1993) and Bogdanova et al. (1996, 2001). According to this scheme, the EEC was formed as a result of Paleoproterozic successive amalgamation of three initially independent crustal segments i.e., Fennoscandia to the northwest, Sarmatia to the south, and Volgo-Uralia to the east (e.g., Bogdanova et al., 2016). Each of the segments is characterised by differences in crustal structure, lithology, and age of crust-forming processes spanning from the Archaean to the Paleoproterozoic (Bogdanova et al., 1996). The Sarmatian crustal segment is built up of several Archaean proto-cratonic terranes formed between c. 3.7 and 2.7 Ga and the Paleoproterozoic belts accreted between 2.2 and 1.9 Ga (Bogdanova et al., 2006). The terranes of Fennoscandia are all younger than 2.0 Ga as they were formed during the Paleoproterozoic Svecofennian orogeny, which involved the accretion of several microcontinents and island arcs (Lahtinen et al., 2009). The crystalline basement of the EEC in Poland belongs to the SW Fennoscandia and the adjacent NW Sarmatia (Fig. 1). The junction between these two amalgamated segments begins in Poland (Fig. 1), where the marginal part of the EEC is bounded to the SW by the TTZ, a tectonic zone separating thinner crust underlying the West European Palaeozoic Platform from the thick crust of the EEC (e.g., Guterch and Grad, 2006, Guterch et al., 2010).

The junction between Fennoscandia and Sarmatia prolongs northeast up to Belarus as the Central Belarus Suture Zone that comprises several tectonically different rock complexes such as the Belarus-Podlasie Granulite Belt (BPGB), Okołowo-Holeszów Belt (OHB), and Ivanovo-Borisov Zone (IBZ) (Fig. 2). The former comprises mostly Palaeoproterozoic (1.90–1.87 Ga) metaigneous, mature-arc-related granulites (Bibikova et al., 1995; Skridlaite and Motuza, 2001; Bogdanova et al., 2006), and

high-grade metasediments (Bogdanova et al., 2001; Taran and Bogdanova, 2003). In contrast, the OHB contains mafic and ultramafic igneous rocks of oceanic island-arc affinity, while the IBZ is composed of juvenile metasediments and metavolcanic rocks dated at c. 1.98 Ga (Bibikova et al., 1995). The south-easternmost EEC basement unit in Poland, the Osnitsk–Mikashevichi Igneous Belt (OMIB) (Fig. 2), represents an active continental margin along the NW edge of Sarmatia developed by Andean-type subduction of oceanic crust at 2.0 – 1.95 Ga (Bogdanova et al., 1996; Claesson et al., 2001). This youngest orogenic belt of Sarmatia contains granitoid massifs emplaced at c. 1.98 to 1.95 Ga as well as inclusions of mafic and felsic metavolcanic and hypabyssal rocks dated at 2.02 Ga (Shcherbak et al., 2002). The NW section of the study area embraces two Fennoscandian crystalline basement units (Bogdanova et al., 2015, 2016): the Mazowsze Domain (MD) and Dobrzyń Domain (Fig. 2).

During the subsequent craton evolution, the suture between Fennoscandia and Sarmatia underwent reactivation by faults bounding the various belts and domains that were inferred as related to post-collisional extensional tectonics between c. 1.80-1.74 Ga and 1.71-1.67 Ga (Bogdanova et al., 2006). The suture zone was also overprinted by the Meso-Neoproterozoic Volhyn–Orsha Aulacogen that occupies the area, where the magnetic reconnaissance (Skridlaite and Motuza, 2001; Petecki and Rosowiecka, 2017; Milano et al., 2019) has indicated the presence of large lens-shaped, mainly NE-trending structures in the crystalline basement (Fig. 3).

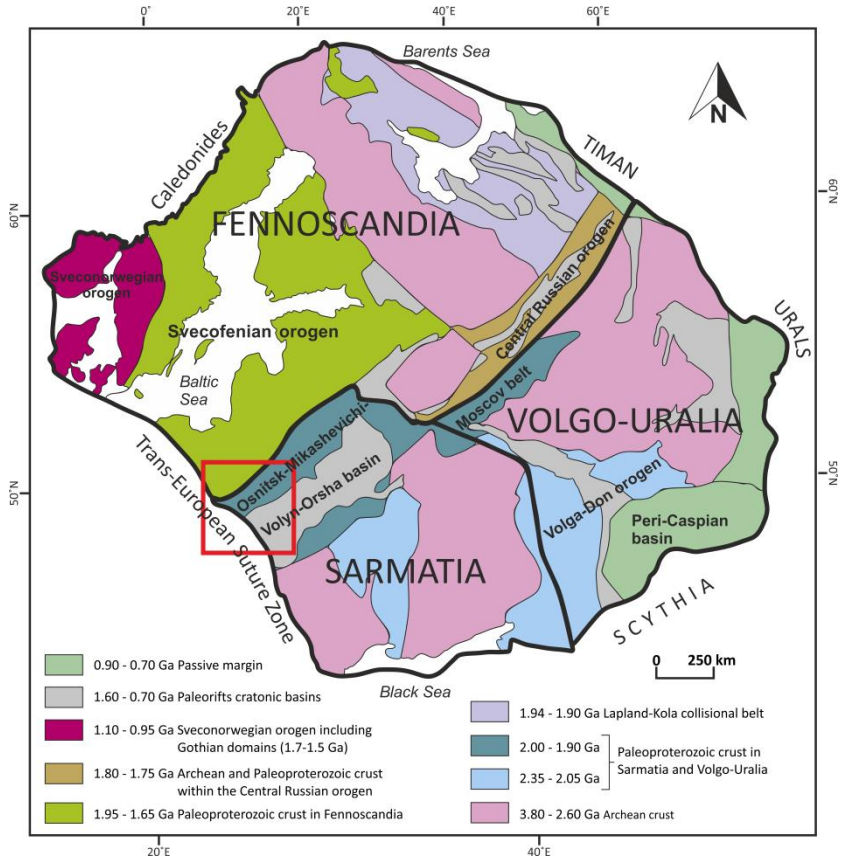

Figure 1. Precambrian tectonic complexes of the East European Craton. The red rectangle shows the study area. Modified from Bogdanova et al. (2016).

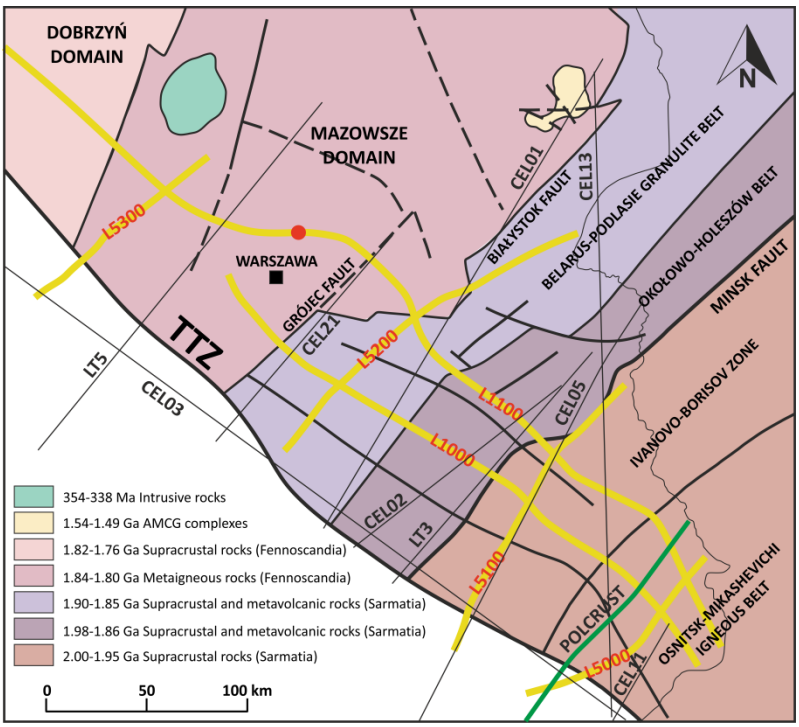

Figure 2. Location of the PolandSPAN™ seismic profiles (yellow lines) on the background of a simplified geological map of the East European Craton crystalline basement units (after Krzemińska et al., 2017). TTZ – Teisseyre–Tornquist Zone. Locations of WARR profiles CEL01, CEL02, CEL03, CEL05, CEL11, CEL13, CEL21, LT3, and LT5 are marked as thin black lines. The red dot indicates

where the part of the profile 1100 analysed in this study begins. The location of the POLCRUST-01 deep reflection seismic profile (Malinowski et al., 2013) is marked in green.

Concurrently with the crustal extension, the magmatism, retrograde metamorphism as well as the emplacement of large AMCG plutons at 1.80-1.74 Ga in Sarmatia, and between c. 1.6 Ga and 1.50 in Fennoscandia substantially influenced the structure of the accreted Palaeoproterozoic terranes and generated a high-velocity layer at the base of the crust (Bogdanova et al., 2006).

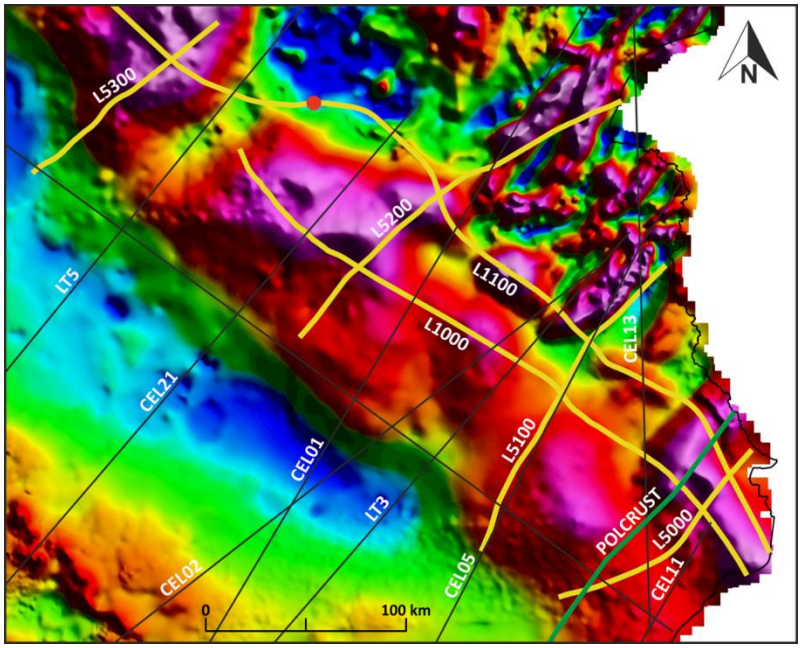

Figure 3. Location of the PolandSPAN™ seismic profiles on the background of a total magnetic field anomaly map of SE Poland (reduced to pole) (data compilation by S. Mazur).

3. Data and methods

3.1 Processing

In this paper, a subset of five PolandSPAN™ profiles (three dip ones: 5000, 5100, 5200 and two strike ones: 1000, 1100) with a total length of ~ 1000 km, transecting major geological units in SE Poland, was reprocessed based on the extended-correlation method of Okaya and Jarchow (1989). Please note though, that in the following only four profiles are presented (5100, 5200, 1000, 1100), since the profile 5000 is relatively short, as well as it coincides with the already interpreted POLCRUST-01 profile (Malinowski et al. 2013, 2015). Acquisition parameters and the full processing sequence have been already described in the earlier study (Mężyk et. al, 2019) and here we follow the same workflow. In brief, prior to regular seismic processing, the raw data were correlated with a ground

force averaged for every Vibroseis point (VP) in order to increase the nominal record length from 12 to 22 s. The correlation process compressed the recorded raw data preserving the full bandwidth (2-150 Hz) for the original record length but limiting a maximum frequency to 57.5 Hz at 22 s of extended time. Further on, we repeated the previously established processing sequence that was focused on the middle to lower crust and the upper mantle depths. It included, among others, the estimation of the refraction static corrections based on the first-break picks derived with an in-house neural-network-based algorithm (Mężyk and Malinowski, 2019). For the NMO-DMO corrections, we used original ION Geophysical root-mean-square (RMS) velocity models after pre-stack time migration (PSTM). After the DMO stack, the coherence of the signal along the seismic sections was considerably improved with a tuned linear dip filtering (Calvert, 2004). Finally, we migrated the data with a simple F−K (Stolt) algorithm and converted the final result to the depth domain. A velocity model for depth conversion was merged from two different sources along the interpreted basement reflector: the pre-stack depth migration (PSDM) velocities provided by ION Geophysical for the upper section and the crustal velocity model for Poland derived from WARR data (Grad et al., 2016) for the lower section.

3.2 **Clustering of seismic reflectivity patterns**

Conventional seismic attributes play an important role in detecting and characterizing the geological structures in the subsurface (Marfurt, 2018). However, the growing number of proposed attributes might pose a problem in deciding which of these attributes are best applied in the particular case or even if they are mutually independent (see e.g. Infante-Paez and Marfurt, 2019). The problem is even more complex when one interprets large datasets (e.g. long 2D regional crustal-scale profiles), which require a series of manual adjustments to match the expected amplitude range of bandlimited reflectivity for visualisation and interpretation purposes. It might be the reason, why seismic attributes are only rarely used in the interpretation of crustal-scale reflection seismic data (Torvela et al., 2013). Here we evaluate the possibility of the automatic classification of crustal reflectivity patterns based on seismic attributes and unsupervised clustering. Our workflow is outlined in Fig. 4 and consists of the following steps.

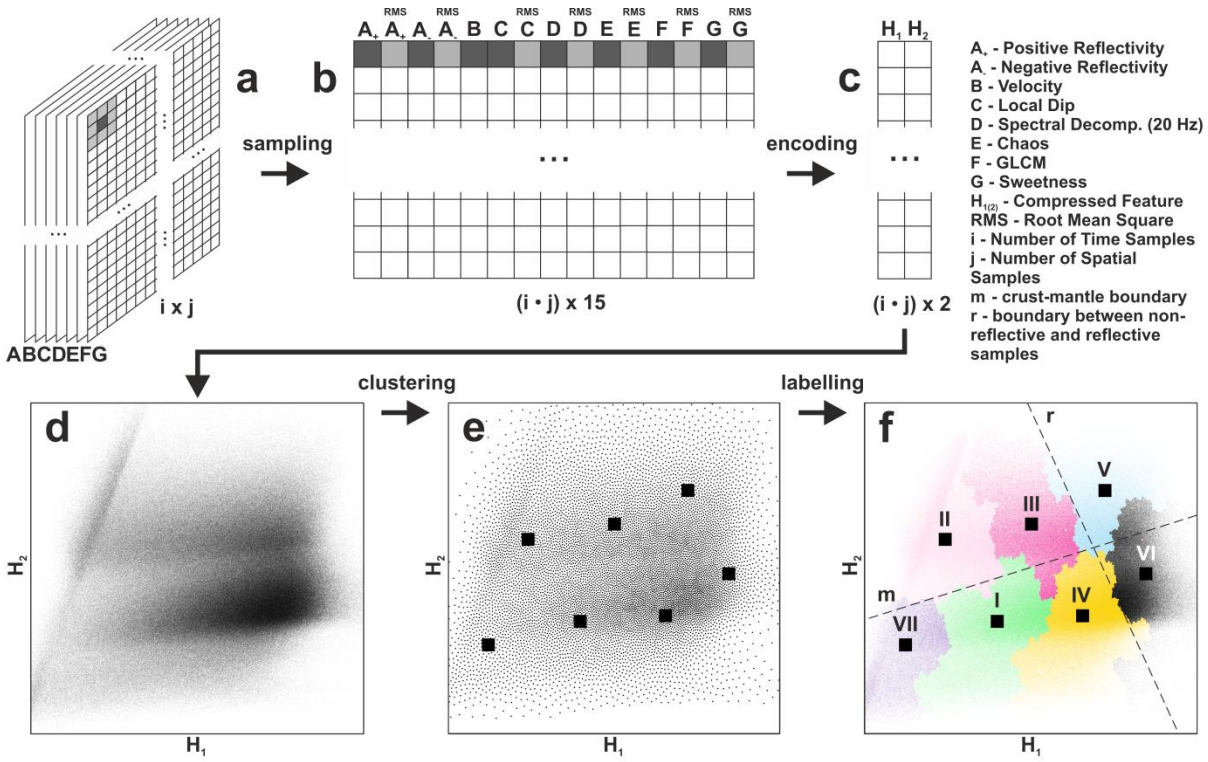

Figure 4. Flow diagram illustrating an unsupervised clustering of crustal reflectivity patterns based on seismic attributes. (a) Set of data matrices containing seismic data and their derivatives (B-G). (b) Combined feature matrix constructed by placing all amplitude and attribute values column-wise. (c) Feature matrix of (b) that underwent the compression using deep learning. (d) Planar representation of the deep-embedded features. (e) Planar representation of cluster centroids obtained with two-step clustering approach. Dots correspond to the location of k-means centroids that are consecutively fed into a hierarchical clustering algorithm to determine the major centroids (rectangles). (f) Scatter plot of (d) after cluster allocation using the centroids derived in (e).

First, we perform conventional seismic attribute analysis to select a few attributes that are valuable in the context of the significant and coherent anomalies they highlight (Fig. 4a, data matrices A-G). Towards this end, we select the following properties: seismic amplitude separated into positive and negative parts, chaos or seismic disorder attribute (Chopra and Marfurt, 2016a), Grey-Level Co-occurrence Matrix (GLCM; West et al., 2002; Di and Gao, 2017), local structural dip, spectral decomposition at 20 Hz (Chopra and Marfurt, 2016b), and sweetness (Hart, 2008). The selected features not only provide basic information on seismic energy and frequency content but are also helpful in examining the reflectors' geometry, continuity, and shape at different scales. We also consider the seismic velocity used for the depth-conversion as a separate attribute. Then, we create a combined feature matrix (Fig. 4b) in such a way that for each i-th sample from the j-th seismic trace and each feature (attribute) we collect two values: the actual value (dark grey in Fig. 4b) and an RMS

value averaged over a 3x3 window centred at this matrix element (light grey in Fig. 4b). Such conditioning improves the data representation. Please note, that we do not compute RMS values for the velocity field as it is already smooth enough. Therefore, each i-th sample is described by fifteen different values (features) corresponding to eight seismic attributes. Subsequently, the feature matrix undergoes the standardization and scaling process to be encoded (through the deep-neural network) into the dimensionally-reduced feature matrix composed of only two embedded components (Fig. 4c, H_1 and H_2 components). Then, we retain only those samples of the H_1 and H_2 components that are located below the crystalline basement and perform a two-step unsupervised clustering. Initially, the encoded data are fed into the k-means algorithm (Jain, 2010) in order to reduce the number of processed samples by defining a large number of data groups (here we use ten thousands) gathering the samples that are most similar in terms of the embedded feature values (Fig. 4e, black dots). The k-means algorithm is suitable for clustering large datasets, but it tends to output relatively even-sized clusters, which we find as a suboptimal final solution to our problem concerning the grouping of seismic data that are locally very heterogeneous. Thus, to efficiently derive the main clusters that are not affected by random initialization and differ in the number of sample members, we consider the x- and y-coordinates of the cluster centroids established in the first step as our new set of features to be clustered again with agglomerative hierarchical clustering (AHC) algorithm (Day and Edelsbrunner, 1984). We determine the appropriate number of the main superclusters (here we aim for seven of them) by analysis of the series of clustering results and their dendrograms illustrating how the larger clusters evolve by the successive merge of sub-clusters. The combination of these two clustering methods allows for fast and reproducible segmentation of seismic sections, even if data volumes (i.e. feature matrices) are large (such as in the case of PolandSPAN™ data). Moreover, the multi-step clustering routine can be easily implemented with open-source machine learning libraries, like for instance scikit-learn (Pedregosa et al., 2011), and modified with other available clustering algorithms besides k-means. More details on the implementation of our algorithm can be found in Mężyk and Malinowski (2020). Once the two-step grouping is completed, each seismic sample is assigned to a certain supercluster. When it comes down to the final plotting, the replacement of amplitudes in the seismic section with the supercluster's membership number allows to highlight the crustal-scale reflection distributions and investigate the complexity of geological structures better across the seismic

profiles without tedious tweaking of amplitude limits for visibility purposes. Fig. 5 shows how the separability of clusters can be used as both visual and quantitative aid for the characterization of different portions of the seismic section regarding the used features and their distributions. What is more, the incoherent reflectivity can be discarded in the clustered sections indicating denoising capabilities of clustering when applied to seismic data (cluster VI in Fig. 5 can be considered as a denoised or reflection-enhanced section).

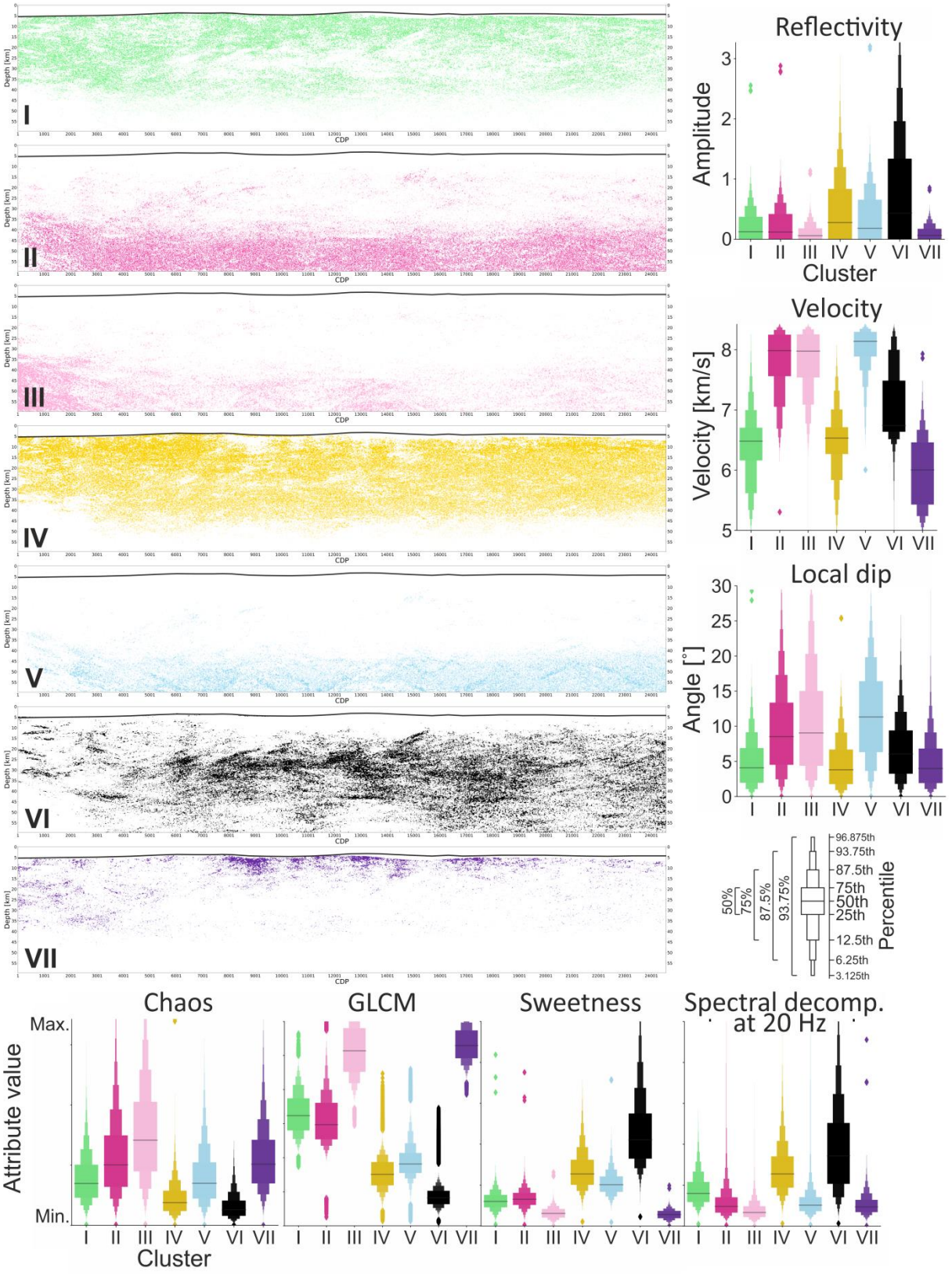

Figure 5. Cluster decomposition on the example of the line 1100. The seismic samples belonging to each of the main clusters (denoted as Roman numerals) are plotted on the individual seismic sections in different colours by replacing the amplitude values with the corresponding cluster membership variables. The black horizontal lines along the clustered sections represent the interpreted sedimentary basement and delimit the clustering analysis above. The box plots represent the distribution of seismic attribute values for each cluster.

It is also feasible to characterize the seismic samples within a single defined cluster in a similar way as shown in Fig. 5 by rerunning the two-step clustering procedure of the initial feature matrix limited to the samples that constitute the selected cluster, like for instance the cluster VI representing the most reflective and useful part of the data used in this study.

4. Results

The final migrated depth-converted sections are presented in Figures 6 – 9 with a smoothed amplitude envelope as a colour background. The latter along with the corresponding results of clustering aims to enhance the information on the printing scale of the sections and facilitate interpretation. As a whole, the reprocessed profiles illustrate broad regional patterns of reflectivity from the uppermost crust to the base of crust including dipping mantle reflections. The relative lateral continuity of deep reflections as well as the signal penetration limit was inferred from the amplitude decay curves generated for samples classified under the reflectivity cluster VI (Fig. 4 and 5). Subsequently, the computed curves were grouped in terms of their crustal affinity (according to the tectonic sub-division presented in Fig. 2) and pre-processed by RMS averaging to produce curves representing the mean amplitude decay within five different crystalline basement units (Fig. 10 a-b). Besides the amplitude decay curves, we present the corresponding depth-distributions of samples averaged in 1 km intervals that constitute the cluster VI (Fig. 10 a'-b'). These distributions allow to assess the overall reflection content at various depth levels and perform the comparative analysis between various crustal units, irrespective of the amplitude levels/thresholds. In the following, we provide an overview of the main features observed in the collected data.

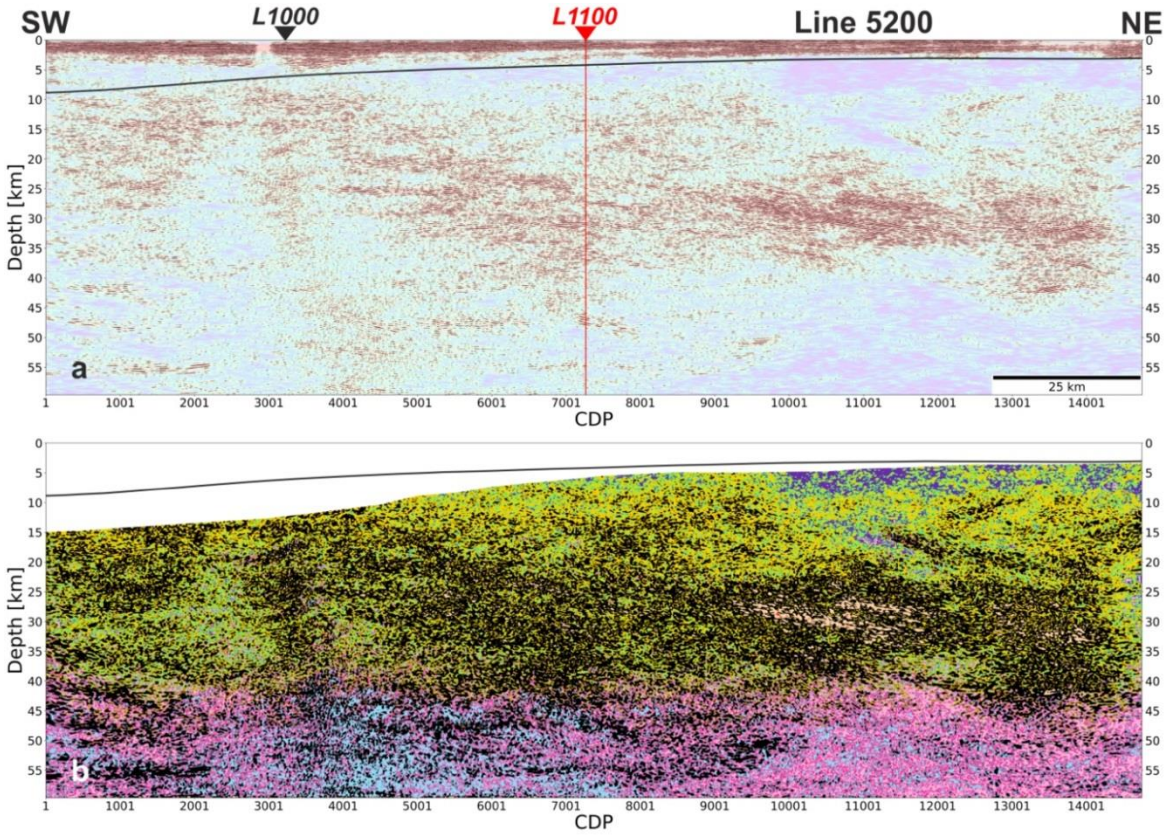

Figure 6. Final migrated depth-converted section along PolandSPAN™ profile 5200. (a) Plot of positive amplitudes with amplitude envelope attribute in the background; (b) Plot of clustered reflectivity section, where samples were replaced with the cluster's membership number. Colours correspond to clusters shown in Fig. 4 and 5.

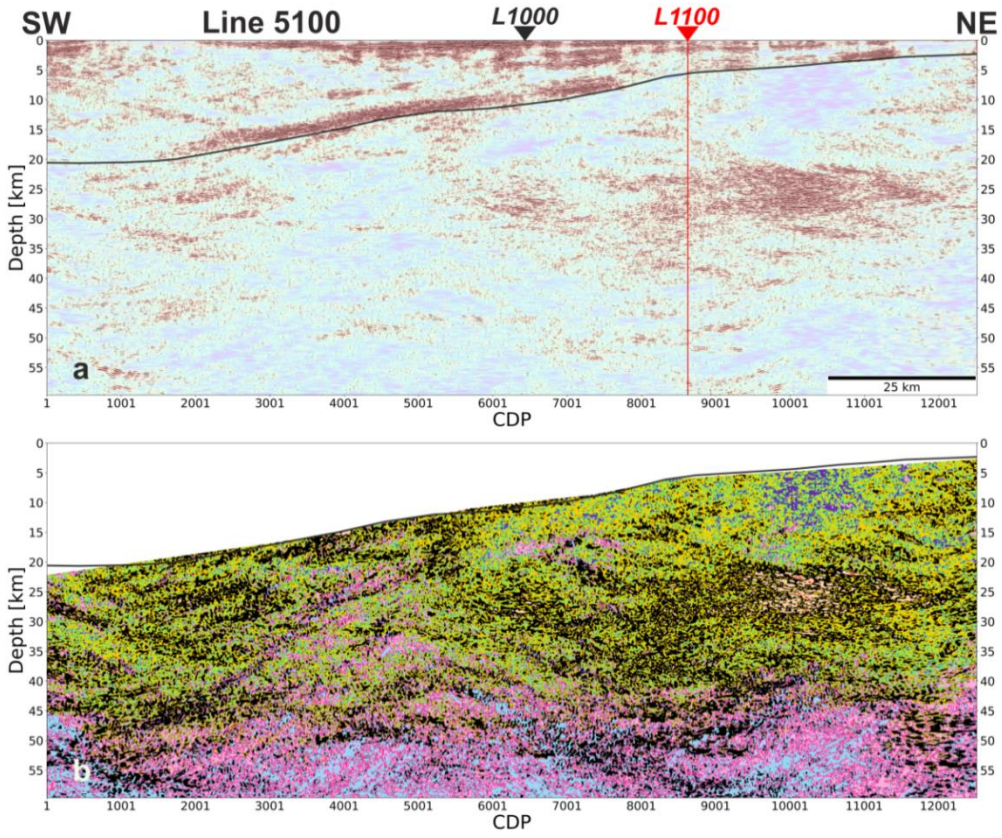

Figure 7. Final migrated depth-converted section along PolandSPAN™ profile 5100. (a) Plot of positive amplitudes with amplitude envelope attribute in the background; (b) Plot of clustered reflectivity section, where samples were replaced with the cluster's membership number. Colours correspond to clusters shown in Fig. 4 and 5.

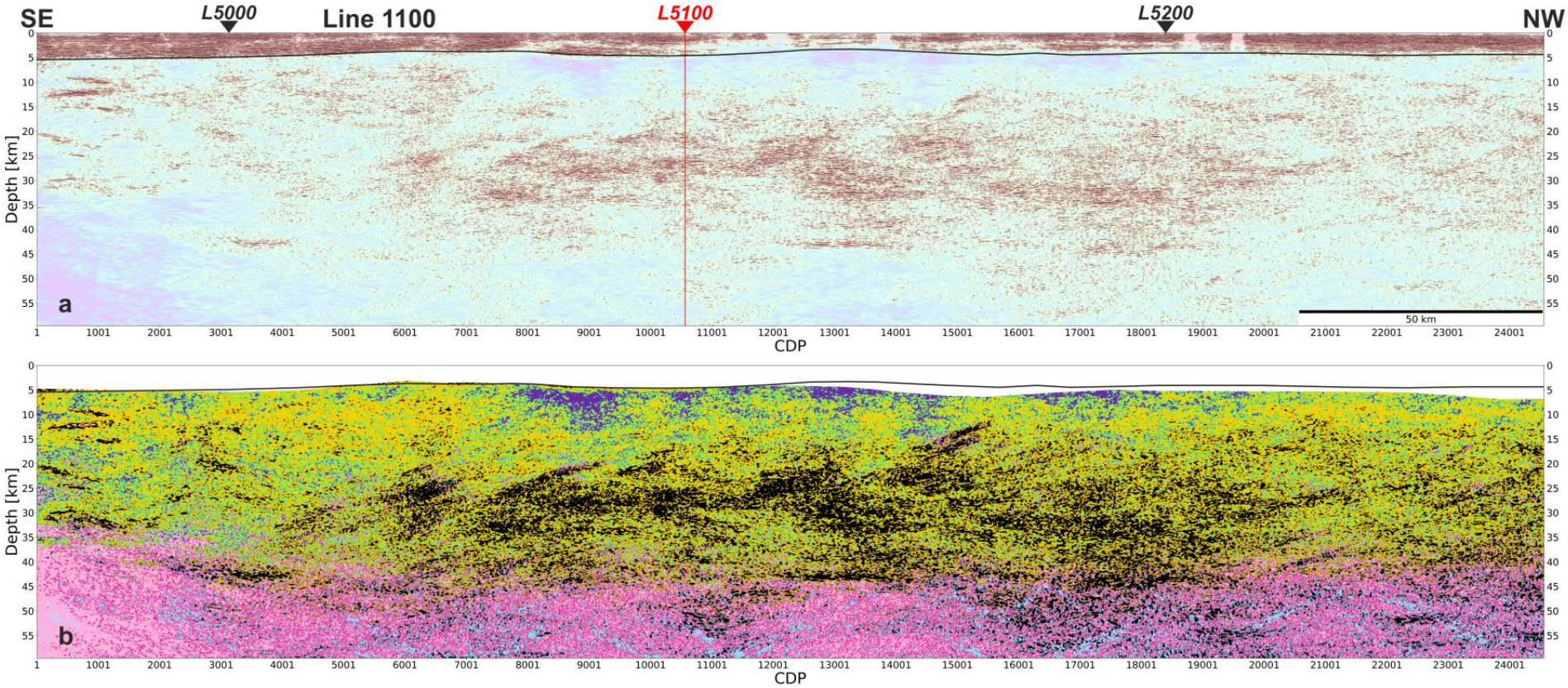

Figure 8. Final migrated depth-converted section along PolandSPAN™ profile 1100. (a) Plot of positive amplitudes with amplitude envelope attribute in the background; (b) Plot of clustered reflectivity section, where samples were replaced with the cluster's membership number. Colours correspond to clusters shown in Fig. 4 and 5.

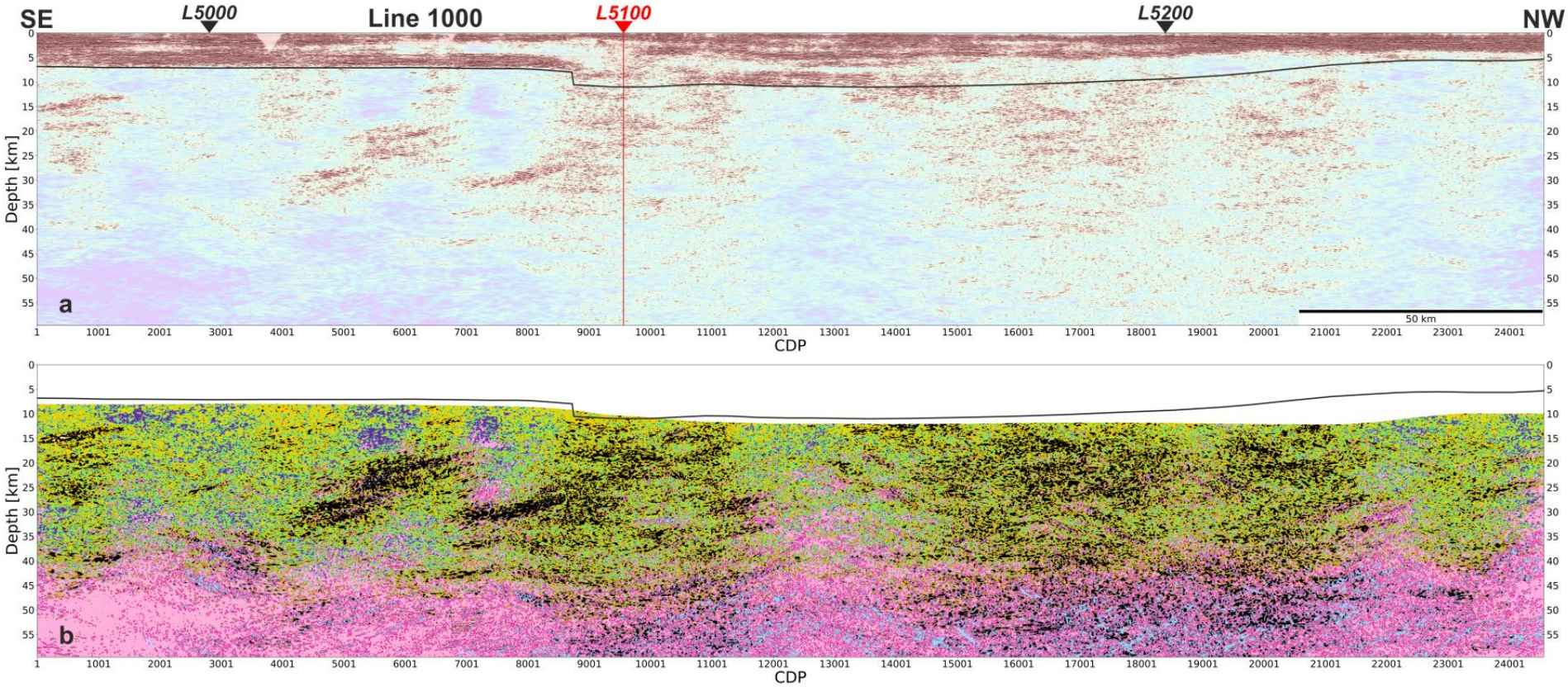

Figure 9. Final migrated depth-converted section along PolandSPAN™ profile 1000. (a) Plot of positive amplitudes with amplitude envelope attribute in the background; (b) Plot of clustered reflectivity section, where samples were replaced with the cluster's membership number. Colours correspond to clusters shown in Fig. 4 and 5.

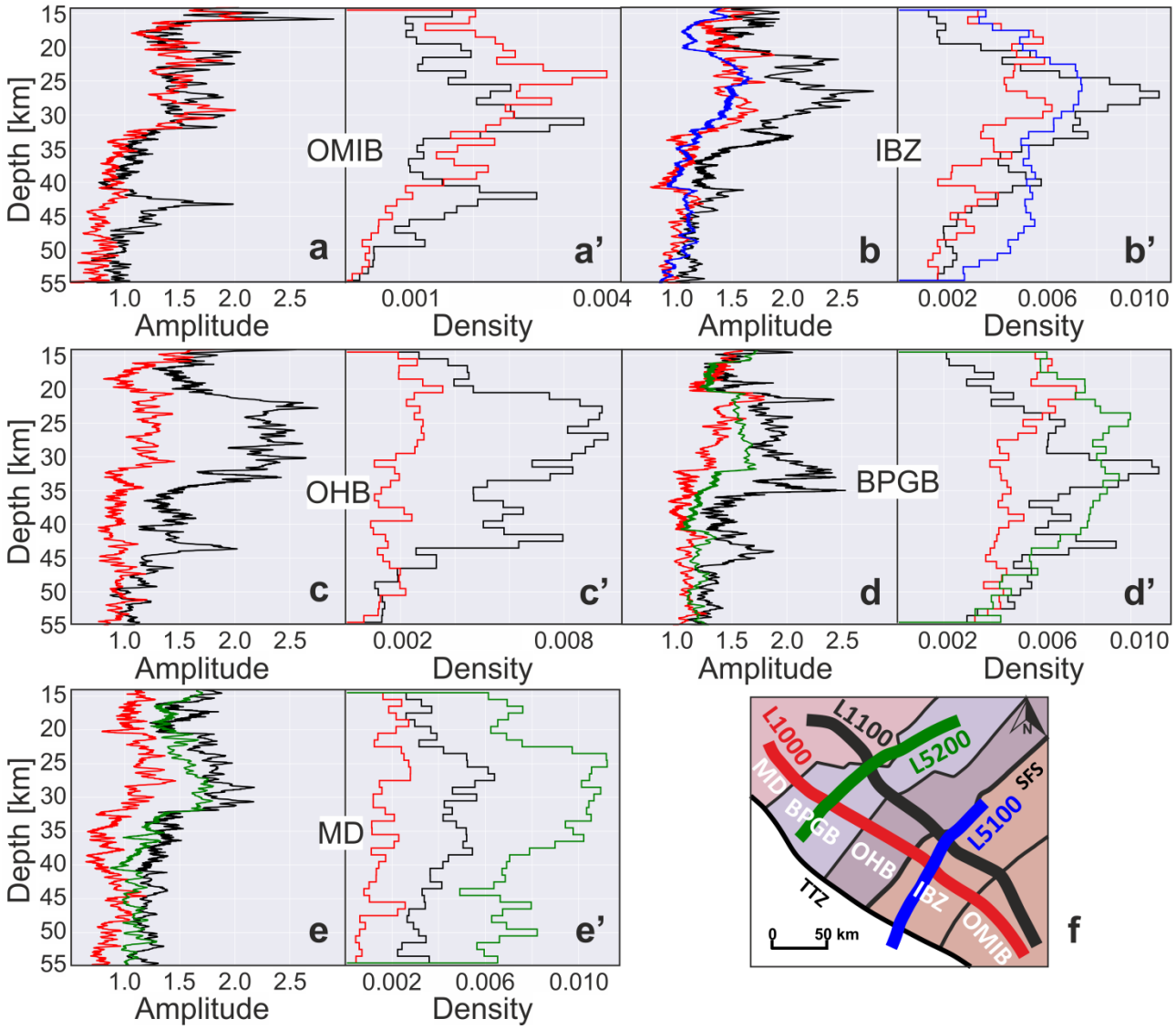

Figure 10. Amplitude decay curves (a – e) and relative frequency distributions (a' – b') extracted from the seismic samples classified under the cluster VI (Fig. 4, 5 and 6b – 9b). Letter and letter-prime symbols represent the data associated with the same crustal units depicted in (f). The colour of curves corresponds to the seismic profiles, whose locations are also shown in (f). Relative frequency (density) is defined as the ratio of the samples belonging to cluster VI to the total number of samples assigned to the given crustal unit and depth interval. It expresses the concentration of desired data points along the 1 km depth intervals.

The upper crust reflectivity is dominated by dense sedimentary reflectors and an acoustically strong basement. Their continuity is considerable and maintained almost entirely along the transects with some exceptions (e.g., 5100 at SW dipping sedimentary basement and CDP 8000-10500, Fig. 7). These strong upper crustal reflectors are also accompanied in places by large poorly reflecting or even transparent zones mostly below the sedimentary basement (e.g. 5200 at 4-8 km and CDP 10000-14750, Fig. 6; 5100 at 5-11 km and CDP 9500-11000, Fig. 7; 1100 at 5-8 km and CDP 7500-20000, Fig. 8). The distribution of the values of the different attributes (features) in various clusters (Fig. 5) also indicates low textural uniformity within those zones, due to the high GLCM energy and chaos value. The mid-to-lower crust exhibits more

diffuse reflection patterns that vary in terms of their intensity and configuration. The sharp reflectors are less frequent and start to be discontinuous at these depths, but they are not chaotic. In the clustered sections, the mid-to-lower crustal reflectivity constitutes the majority of samples classified under the black-coloured cluster VI that features strong and intermittent reflections with a high content of frequency around 20 Hz (Fig. 5). In the 5200 profile, they tend to consistently dip in the NE direction (opposed to the sedimentary basement) at an angle around 12 degrees until they reach a highly reflective zone, where they flatten out (Fig. 6). The presence of these zones, marked in a depth range of 20 to 35 km, is even more pronounced as they are located just below the aforementioned transparent spots. It is also worth noticing that they are in close vicinity of the areas, where the profiles 5200 and 5100 crosses with the strike profile 1100. The latter is characterized by a rich collage of mid-to-lower crustal reflections that can be followed across a 200-km long segment in the centre of the profile 1100. Within this segment, once again we observe the change from SE dipping to subhorizontal reflectors extended over a larger area (Fig. 8). The analysis of the overall intracrustal configuration of reflectivity in the profile 1000, parallel to the line 1100, shows large acoustically-transparent zones that prolong from the sedimentary basement to the deeper parts of the section, indicating a gradual transition from crustal to mantle rocks. Besides that, the reflectors of the profile 1000 seem to dip towards the southeast with a tendency to level off slightly to the north. The transition between the generally reflective lower crust and the transparent uppermost mantle (e.g. 1100 at CDP 8000-9000, Fig. 8) or the band of stronger reflectivity (e.g. 1100 at CDP 12000-14000, Fig. 8) allows for delineation of the Moho boundary that undulates between 40 and 48 km in SE Poland and indicates a sudden reflectivity drop. The Moho can also be inferred from the amplitude decay curves and the distributions of the samples within the cluster VI as a highly noticeable temporary deviation in amplitude and relative frequency, respectively, in the depth interval from 40 to 45 km (Fig. 10). However, due to insufficient signal penetration, the amplitude signature of the crust-mantle transition zone might be very subtle or hardly distinguishable, like for instance in the amplitude decay curve calculated for the IBZ or MD unit (Fig. 10 b and e, respectively). The Moho-related effects that are seen on the relative frequency distributions of samples classified as reflective ones (cluster VI) (Fig. 10 a'-b'), except for the distribution calculated for the MD, expose a significant decline in the number of these samples at a depth of c. 45 km. In general, the histograms show a rapid increase in the number of samples belonging to cluster VI (most pronounced reflectivity) that continues from the upper crust down to ca. 30 km, whereby it stabilises at the high level and starts to decrease until it reaches the local

minimum placed around depths of 35-40 km that relates to the base of the lower crust just above the Moho discontinuity. It interesting to note here that one-third of the total number of samples classified as strongest reflections (cluster VI) are found both in the depth interval of 15-30 km and 30-45 km. Although the explicit depletion in reflectivity is expected below the Moho, the relative frequency of reflections within the BPGB crustal unit is the highest when compared to other units. As far as the sub-Moho reflectivity is concerned, the stronger and dipping reflectors (e.g. 5200 at CDP 1000-2000, Fig. 6; 1100 at CDP 22000-23000, Fig. 8; 1000 at CDP 19000-21000, Fig. 9) seem to be real, but the hyperbolic ones are most likely related to processing footprints (e.g. migration artefacts). Furthermore, the cluster analysis at this depth reveals a group of weak and steeper reflections (outlined in light blue in Figs. 6 – 9b) that, for instance, might be evidence for the residue of ancient subduction within the upper mantle.

5. Interpretation and discussion

To understand the geometry of the Paleoproterozoic Sarmatia-Fennoscandia Suture (SFS) at the SW margin of the EEC, four PolandSPAN^{TM} seismic profiles (5100, 5200, 1000, 1100) were utilized for the structural interpretation supported by overall geological and geophysical information, referred to in the previous sections. These interpreted profiles (Figs. 11 – 12) show that the deep structure of the EEC at the suture zone fundamentally differs from a 'simple' three-layered crystalline crust inferred from the WARR compilation by Majdański (2012). When combined with the consistently reprocessed and already published PolandSPAN^{TM} profiles in NE Poland (Mężyk et al., 2019), they allow for a comprehensive redefinition of previously established crustal models in the marginal part of the EEC.

In the convergence area, the oblique collision of Sarmatia and Fennoscandia resulted in a widespread NNW-vergent transpression that in turn led to kinematically complex re-arrangement of the Archean and Paleoproterozoic upper lithosphere (Bogdanova et al., 2005a; Lahtinen et al., 2005). According to the previous studies (Bogdanova et al., 1996, 2006; Taran and Bogdanova, 2001), the boundary between these two crustal segments is defined by a major lithospheric discontinuity in the EEC – the Minsk Fault (Fig. 2). The seismic images in this paper, however, show no evidence of a such large thrust-like structure in SE Poland that would extend to the Moho or explicitly separate the amalgamated crustal units. Instead, we observe a so-called diffuse cryptic suture zone, where materials from two colliding plates are mixed together

over large distances to form a unified continental crust. A similar type of collision zone, formed as the result of the Trans-Hudson Orogeny, was already recognized in the Canadian Shield by White et al. (2005). In SE Poland, it is especially well illuminated on the profiles perpendicular to the N and NNE-trending shear zones, i.e. profiles 1000 & 1100 (Fig. 12). The analysis of reflection packages along the latter with regard to their crustal affiliation indicates that lithospheric shortening intensively affected the units straddling the boundary between Fennoscandia and Sarmatia– the IBZ, OHB, BPGB down to the top of the lower crust. This c. 150 km wide zone represents a series of wedge-shaped blocks of the upper lithosphere that dip to the southeast at a low-angle beneath Sarmatia. The SE polarity of reflections is thought to be a consequence of the SE-directed fossil subduction of an oceanic plate beneath the continental segment of Sarmatia (Taran and Bogdanova, 2001). The relicts of the subducted crust followed by the collisional stacking might have caused the crustal thickening in the vicinity of the SFS, where the lower crust is poorly resolved and some dipping reflections emerge at the depth larger than it can be deduced from interpolation of the adjacent Moho reflections. The SFS zone is surrounded by the most reflective Moho boundary in the all reprocessed profiles, which is seen along the line 1100 in the CDP range 12500 – 14000 and tracked farther south or north at a similar depth (i.e. 43 km). The segment of the line 1100, constrained by the intersections with the lines 5100 & 5200, is characterized by the leading plate margin uplift above the trailing footwall ramp of the Fennoscandian thrust sheet that immediately underlies the Sarmatian plate. This site is also represented by the prominent magnetic anomalies that strike in the NNE direction (Fig. 3) up to Belarus and Baltic countries (Skridlaite and Motuza, 2001). Similar deformation zones dipping to SE were found by Trofimov (2006) in the adjoining Volgo-Uralia crustal segment and explained as the result of the 1.85–1.80 Ga reworking of the Archean and Paleoproterozoic rocks (Bogdanova et al., 2005b).

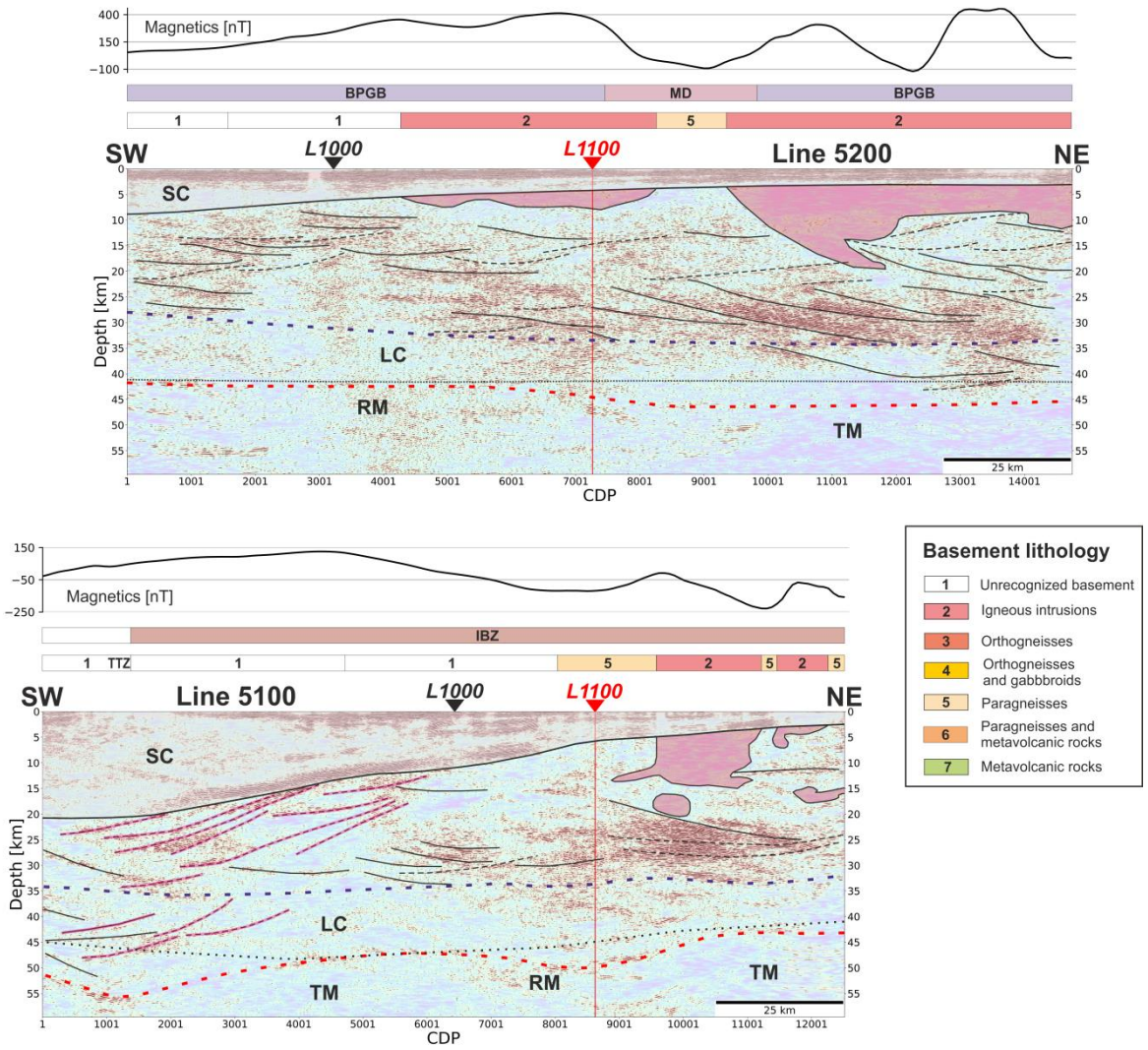

Figure 11. Final migrated depth-converted sections along PolandSPAN™ profile 5100 and 5200 with its tentative interpretation. Bars atop the section are colour-coded according to the crystalline basement lithologies following Krzemińska et al. (2017) (see a legend). The magnetic profile at the top is extracted from the magnetic anomaly map (Fig. 3). The solid and dashed black lines delineate NE dipping major reflection fabrics and some weaker SW dipping crust reflections, respectively, which we infer from the data. SW-dipping reflectors in the SW section of profile 5100, potentially corresponding to low-angle normal shear zones, are highlighted in magenta. The black dotted line is the Moho boundary taken from the WARR compilation by Majdański (2012). The dashed blue and red lines represent the top of the lower crust and Moho boundary, respectively, interpreted from reflection data. BPGB - Belarus-Podlasie Granulite Belt, IBZ - Ivanovo-Borisov Zone, MD – Mazowsze Domain, TTZ - Teisseyre-Tornquist Zone, F – fault.

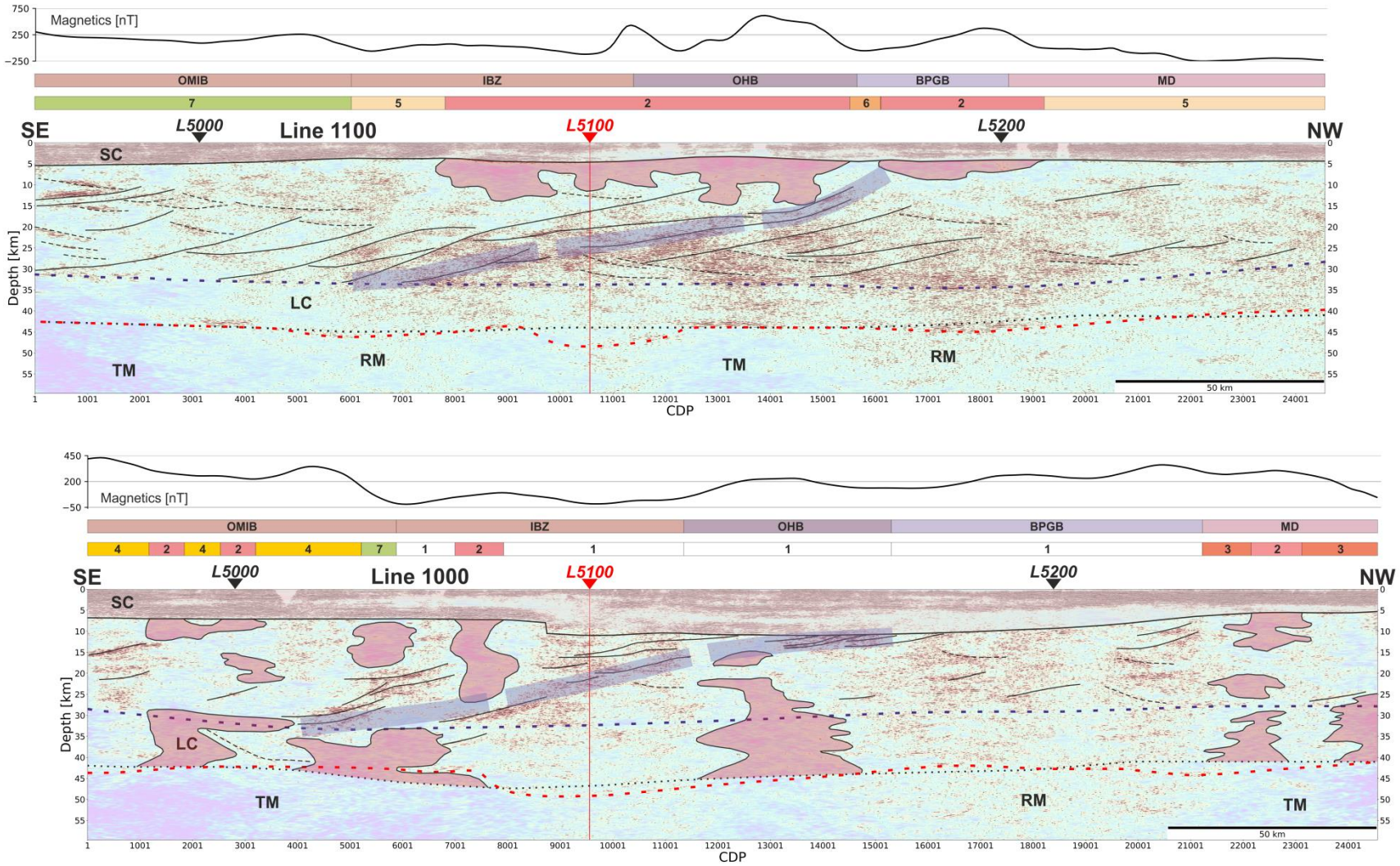

Figure 12. Final migrated depth-converted sections along PolandSPAN™ profile 1000 and 1100 with its tentative interpretation. Bars atop the section are colour-coded according to the crystalline basement lithologies following Krzemińska et al. (2017) (see Fig. 11 for a legend). The magnetic profile at the top is extracted from the magnetic anomaly map (Fig. 3). The solid and dashed black lines delineate SE dipping major reflection fabrics and some weaker NW dipping crust reflections, respectively, which we infer from the data. The potential position of the collisional suture between Sarmatia and Fennoscandia is highlighted in semi-transparent electric blue. The black dotted line is the Moho boundary taken from the WARR compilation of Majdański (2012). The dashed blue and red lines represent the top of the lower crust and Moho boundary, respectively, interpreted from reflection data. BPGB - Belarus-Podlasie Granulite Belt, F – fault, GF – Grójec Fault, IBZ - Ivanovo-Borisov Zone, MD – Mazowsze Domain, OHB - Okołowo-Holeszów Belt, OMIB - Osnitsk–Mikashevichi Igneous Belt, SFS – Sarmatia-Fennoscandia Suture, TTZ - Teisseyre-Tornquist Zone.

Parallel to the suture zone, the dip profiles 5100 and 5200 depict highly reflective concave shapes bounded mostly by the reflectors in the middle crust within the IBZ and the BPGB unit, respectively. What is more, the line 5100 coincide with the refraction profile CEL05 (Fig. 2), along which Grad et al. (2006b) reported the spatial heterogeneity of P-wave velocity within the crust and upper mantle boundary in the close vicinity of the SFS. Although the profiles are c. 100 km apart, their NE parts tend to dip in the common direction at the angle range between 10 and 15 degrees. The puzzling feature of the crust across the SW part of the profile 5100 is another crustal thickening, but this time in the vicinity of the TTZ. The change in the dip of the overall reflectivity might be evidence of crustal stretching related to Ediacaran rifting.

The reprocessed profiles indicate that the crustal thickness in SE Poland varies between 40 and 48 km with a typical value around 43 km, which is slightly higher than the average value of 40 km observed in the northeast PolandSPAN^{TM} data (Mężyk et al., 2019). The interpreted reflection Moho is in good agreement with the WARR Moho (depicted as a red dashed and black dotted line in Figs. 11-12, respectively), except for a few instances. The largest discrepancy occurs in the intersection of the line 1100 with the dip profiles as well as in the vicinity of the TTZ along the line 5100. However, it should be stressed here that we used reflection-derived velocities at shallower depths in the time-to-depth conversion to accommodate the poorly resolved sedimentary cover in WARR models. The Moho boundary is also visible at a depth of c. 45 km as the instant drop in the number of the reflections extracted and grouped according to their crustal affinity in the clustering process (Fig. 10b). The distribution of these histograms indicates the major accumulation of reflectivity in the middle crust, which is surprisingly similar to the histogram of reflection density obtained for the average metamorphic-assemblage crust by Christensen and Mooney (1995, their fig. 18). The authors stated that the abundance of the major reflections at mid-crustal depths originated in their case from the large contrasts in acoustic impedance of amphibolite vs granitic gneiss and tonalitic gneiss. According to Bogdanova et al. (2006), lower crustal granulites underwent juxtaposition with upper and mid-crustal amphibolite-facies rocks in the region between the Baltic and Ukrainian shields. The presence of the granulites instead of the gneisses in the lowermost crust of the EEC overlain by amphibolites might still pose a highly reflective boundary and be an explanation for the anomaly in the described

histograms. Furthermore, the comparative analysis of the distribution curves shows the shallower peak of the reflectivity in the upper OHB crust (Fig. 10b), which can be inferred to indicate the location of the uplift in the leading margin of the Sarmatian plate and mark the termination of the SE dipping thrust-wedge in the upper crust.

Our seismic data are inconsistent with the Minsk Fault (dividing the OHB and IBZ; Fig. 2) as a localised suture between Sarmatia and Fennoscandia as it was earlier postulated based on the EUROBRIDGE'97 seismic profile (Taran & Bogdanova, 2001; Bogdanova et al., 2001, 2006, 2008; Janutyte et al., 2014). The continuation of such a suture in the territory of Poland would be represented by the Hanna Fault (Krzemińska et al., 2017). We do not support an alternative interpretation either that places the suture farther south, southeast of the Lublin Basin (Narkiewicz et al., 2011). This concept based on the interpretation of the CELEBRATION 2000 seismic experiment points to the NW edge of the so-called Narol Block as the hypothetical suture zone (Narkiewicz et al., 2011). There is a narrow zone of strongly thickened crust, visible in the CEL03 and CEL14 profiles, with the Moho discontinuity below 52 km (Janik et al., 2005). Instead, our seismic data agree with the new model by Bogdanova et al. (2015, 2016), who no longer regard the OHB and BPGB as parts of or closely related to Fennoscandia. The reason is that at 2.0–1.95 Ga the OHB and BPGB underwent an evolution similar to that of the NW margin of Sarmatia (Bogdanova et al., 2015). In profiles 1000 and 1100, the main bundle of reflectors, potentially representing a Paleoproterozoic suture zone, is rooted at the lower-middle crust interface underneath the IBZ (Fig. 12). They gradually ascend upwards throughout the middle and upper crust beneath the OHB and BPGB to reach the top of the pre-Neoproterozoic basement near the boundary between the OHB and BPGB (Fig. 12). Some other reflectors ascend to the base Neoproterozoic unconformity as far north as the boundary between BPGB and MD (Fig. 12). The latter corresponds to the Grodno-Bialystok deformation zone marking a notable discordance between the tectonic domains of Fennoscandia on one side and the BPGB and OHB on the other. Very consistently, the NE-trending Grodno-Bialystok deformation zone, which defines the north-western limit of the BPGP, obliquely truncates the essentially NW-SE-trending array of various Fennoscandian belts and domains, which are bent and displaced in the vicinity of this boundary (Bogdanova et al.,

2015). Integrating the model proposed by Bogdanova et al. (2015) with our seismic data, the entire BPGB and OHB can be considered a diffuse suture between Fennoscandia and Sarmatia.

After the amalgamation of Fennoscandia and Sarmatia about 1.82-1.80 Ga (e.g., Bogdanova et al., 2008, 2015; Shumlyanskyy et al., 2012), the collisional suture between the two was reactivated by a continental rift system (Bogdanova et al., 1996) that played a significant role in the development of the Neoproterozoic sedimentary basin within the Lublin sector of the EEC margin (Poprawa and Pacześna, 2002; Pacześna 2014; Poprawa et al., 2020). In SE Poland and Volyn, Neoproterozoic rifting was accompanied by volcanism that produced lava flows and pyroclastic rocks revealing the geochemical signature of continental basalts (Pacześna, 2014). Volcanic eruptions occurred between 588.0 ± 8 Ma and 551.0 ± 4 Ma, judging from syn-eruptive zircons, together with zircons recycled from previous ash falls (Poprawa et al., 2020). Rifting developed along both the SW margin of incipient Baltica (Tornquist Rift) and the Orsha-Volyn Aulacogen (Poprawa et al., 2020). A coincidence of the latter with the Paleoproterozoic SFS supports contemporary hypotheses about the effect of deep lithospheric heterogeneity on the distribution and character of deformation in the interior of continents (e.g., Heron et al., 2016). The results of numerical experiments suggest that collisional sutures, conserved in the lithosphere of cratons, can act as pseudo plate boundaries being reactivated by far-field horizontal stress transferred from current plate boundaries (Heron et al., 2016). Although, our seismic data do not reveal any direct evidence for extension associated with the SW termination of the Orsha-Volyn Aulacogen the probable SFS reaches the top of the crystalline basement at the same point, where Krzywiec et al. (2018) postulated the occurrence of an Ediacaran NE-SW-trending graben. This offers a possibility that the SFS was reactivated by Neoproterozoic continental rifting as a pre-existing crustal weakness zone. In addition, a set of SW-dipping reflectors in the SW section of profile 5100 (Fig. 11) may correspond to low-angle normal shear zones related to rifting of Rodinia and break-up of the Tornquist Ocean.

6. Conclusions

The reprocessed regional seismic profiles from the PolandSPAN™ project and their interpretation, showing the SFS in SE Poland, provide the following conclusions. (1) The Paleoproterozoic collision

between Sarmatia and Fennoscandia led to the formation of a cryptic and diffuse crustal suture represented by a c. 150 km wide deformation zone. The suture-related reflections are interpreted as a thrust-wedge rooted at the lower-middle crust interface underneath the IBZ crustal unit and ascending upwards until the top of the pre-Neoproterozoic basement near the boundary between the OHB and BPGB is reached. (2) The integration of our seismic data with the most recent model proposed by Bogdanova et al. (2015) supports the interpretation according to which the OHB and BPGB show affinities to the NW margin of Sarmatia and correspond to a diffuse suture between Fennoscandia and Sarmatia. (3) A novel method of clustering seismic reflectivity patterns based on seismic attributes contributed significantly to the above interpretation. By segmenting seismic samples into distinct groups, it is possible to quantify differences in reflectivity of the desired portions of data and eliminate those which obstruct the interpretability of seismic images. Moreover, data separability provides complete control over the visual layout of section plots and facilitates comparative analysis of key seismic properties and their distributions along the processed profiles.

Acknowledgments

This study was funded by the Polish National Science Centre grant no UMO-2015/19/B/ST10/01612. We are grateful to A. Calvert for sharing his coherency filtration and segment migration codes with us. We are indebted to ION Geophysical for permission to use and show PolandSPAN™ data. Processing was done using GlobeClaritas™ software under the license from Petrosys Ltd. Seismic attributes were calculated using Schlumberger Petrel software donated under the academic software grant. Also, we would like to thank the scikit-learn developers for actively developing and maintaining this open-source tool. Comments from the Editor (N. Lubnina), T. Fomin, and an anonymous reviewer are greatly appreciated.

References

BABEL Working Group, 1993. Deep Seismic Reflection/Refraction Interpretation of Crustal Structure Along Babel Profiles A and B In the Southern Baltic Sea. Geophys. J. Int., 112, 325–343.

Bibikova, E. V., Bogdanova, S. V., and Gorbatschev, R. M., 1995. Isotopic Age, Nature, and Structure of the Precambrian Crust in Belarus. Stratigr. Geol. Korrelyatsiya 3(6), 68–78.

Bielik M., Kloska K., Meurers B., Švancara J., Wybraniec S., Fancsik T., Grad M., Grand T., Guterch A., Katona M., Królikowski C., Mikuška J., Pašteka R., Petecki Z., Polechońska O., Ruess D., Szalaiová V., Šefara J., Vozár J., 2006. Gravity anomaly map of the CELEBRATION 2000 region. Geologica Carpathica, 57(3), 145–156.

Bogdanova, S.V., 1993. Segments of the East European Craton. In: Gee, D.G., Beckholmen, M. (Eds.), EUROPROBE in Jablonna 1991. European Science Foundation, Polish Academy of Sciences, pp. 33–38.

Bogdanova, S. V., Bingen, B., Gorbatschev, R., Kheraskova, T. N., Kozlov, V. I., Puchkov, V. N., & Volozh, Y. A., 2008. The East European Craton (Baltica) before and during the assembly of Rodinia. Precambrian Research, 160(1-2), 23–45.

Bogdanova, S.V., Paskhevich, I.K., Gorbatchev, R., Orlyuk, M.I., 1996. Riphean rifting and major Paleoproterozoic crustal boundaries in the basement of the East European Craton: geology and geophysics. Tectonophysics, 268(1-4),1-21.

Bogdanova, S.V., Gorbatschev, R., Stephenson, R.A., 2001. EUROBRIDGE: Palaeoproterozoic accretion of Fennoscandia and Sarmatia. Tectonophysics, 339 (1–2), 39–66.

Bogdanova, S.V., Gorbatschev, R., Garetsky, R.G., 2005a. The East European Craton. In: Selley, R.C., Cocks, L.R., Plimer, I.R. (Eds.), Encyclopedia of Geology. Elsevier, 34–49.

Bogdanova, S., De Waele, B., Bibikova, E., Postnikov, A., Popova, L., 2005b. Volgo-Uralia: SHRIMP evidence of strong Paleoproterozoic reworking of the Archean crust: Supercontinents and Earth Evolution Symposium: Fremantle, Western Australia, Geological Society of Australia, Abstracts no. 81, p. 118.

Bogdanova, S., Gorbatschev, R., Grad, M., Janik, T., Guterch, A., Kozlovskaya, E., Motuza, G., Skridlaite, G., Starostenko, V., Taran, L., Eurobridge and Polonaise Working Groups, 2006.

EUROBRIDGE: new insight into the geodynamic evolution of the East European Craton. Geological Society, London, Memoirs, 32(1), 599–625. https://doi.org/10.1144/gsl.mem.2006.032.01.36

Bogdanova, S., Gorbatschev, R., Skridlaite, G., Soesoo, A., Taran, L. and Kurlovich, D., 2015. Trans-Baltic Palaeoproterozoic correlations towards the reconstruction of supercontinent Columbia/Nuna. Precambrian Research, 259, 5-33.

Bogdanova, S., Gorbatschev, R., Garetsky, R. G., 2016. EUROPE|East European Craton. Reference Module in Earth Systems and Environmental Sciences. https://doi.org/10.1016/b978-0-12-409548-9.10020-x

Calvert, A. J., 2004. A method for avoiding artifacts in the migration of deep seismic reflection data. Tectonophysics, 388, 201–212. https://doi.org/10.1016/J.TECTO.2004.07.026

Claesson, S., Bibikova, E., Bogdanova, S.V., Skobelev, V., 2001. Isotopic evidence for Palaeoproterozoic accretion in the basement of the East European Craton, East European Craton. Tectonophysics, 339(1-2), 1-18.

Chopra, S., and Marfurt, K. J., 2016a. Understanding the seismic disorder attribute and its applications. The Leading Edge, 35(8), 695–702.

Chopra, S., and Marfurt, K. J., 2016b. Spectral decomposition and spectral balancing of seismic data. The Leading Edge, 35(2), 176–179.

Christensen, N. I., and Mooney, W. D., 1995. Seismic velocity structure and composition of the continental crust: a global view. J. Geophys. Res., 100, 9761–9788.

Day, W. H., and Edelsbrunner, H., 1984. Efficient algorithms for agglomerative hierarchical clustering methods. Journal of classification, 1(1), 7-24.

Di, H., and Gao, D., 2017. Nonlinear gray-level co-occurrence matrix texture analysis for improved seismic facies interpretation. Interpretation, 5, no. 3, SJ31–SJ40.

Gee, D.G., and Stephenson, R.A., 2006. The European lithosphere: an introduction. In: Gee, D.G., Stephenson, R.A. (Eds.), European Lithosphere Dynamics. Geological Society, 1–9.

Grad, M., Guterch, A., Keller, G. R., Janik, T., Hegedűs, E., Vozár, J., Ślączka, A., Tiira, T., and Yliniemi, J., 2006b. Lithospheric structure beneath trans-Carpathian transect from Precambrian platform to Pannonian basin: CELEBRATION 2000 seismic profile CEL05. J. Geophys. Res., 111, B03301.

Grad, M., Janik, T., Guterch, A., Środa, P. and Czuba, W., 2006a. Lithospheric structure of the western part of the East European Craton investigated by deep seismic profiles. Geological Quarterly, 50(1), pp.9-22.

Grad M., and Polkowski M., 2016. Seismic basement in Poland. Int J Earth Sci, 105(4), 1199–1214. https ://doi.org/10.1007/s00531-015-1233-8

Guterch, A., and Grad, M., 2006. Lithospheric structure of the TESZ in Poland based on modern seismic experiments. Geological Quarterly, 50(1), 23-32.

Guterch, A., Wybraniec, S., Grad, M., Chadwick, R.A., Krawczyk, C.M., Ziegler, P.A., Thybo, H., De Vos, W., 2010. Crustal structure and structural framework. In: Doornenbal, J.C., Stevenson, A.G. (Eds.), Petroleum Geological Atlas of the Southern Permian Basin Area. EAGE Publications, 11-23.

Hart, B. S., 2008. Channel detection in 3-D seismic data using sweetness. AAPG Bulletin, 92(6), 733–742.

Heron, P.J., Pysklywec, R.N., Stephenson, R., 2016. Lasting mantle scars lead to perennial plate tectonics. Nature Communications, 7, 11834.

Infante-Paez, L., & Marfurt, K. J., 2019. Using machine learning as an aid to seismic geomorphology, which attributes are the best input? Interpretation, 1–60. doi:10.1190/int-2018-0096.1

Jain, A. K., 2010. Data clustering: 50 years beyond K-means. Pattern Recognition Letters, 31(8), 651–666. doi:10.1016/j.patrec.2009.09.011

Janik, T., Grad, M., Guterch, A., Dadlez, R., Yliniemi, J., Tiira, T., Keller, G.R., Gaczyński, E., CELEBRATION 2000 Working Group, 2005. Lithospheric structure of the Trans-European Suture Zone along the TTZ–CEL03 seismic transect (from NW to SE Poland). Tectonophysics, 411, 129–156.

Janik, T., Grad, M., Guterch, A., CELEBRATION 2000 Working Group, 2009. Seismic structure of the lithosphere between the East European Craton and the Carpathians from the net of CELEBRATION 2000 profiles in SE Poland. Geological Quarterly, 53(1), 141-158.

Janutyte, I., Kozlovskaya, E., Majdanski, M., Voss, P.H., Budraitis, M., 2014. Traces of the crustal units and the upper-mantle structure in the southwestern part of the East European Craton. Solid Earth, 5, 821–836.

Juhlin, C., Stephenson, R.A., Klushin, S., 1996. Reappraisal of deep seismic reflection profile VIII across the Pripyat Trough. Tectonophysics, 268, 99-108.

Krzemińska, E., Krzemiński, L., Petecki, Z., Wiszniewska, J., Salwa, S., Żaba, J., Gaidzik, K., Williams, I.S., Rosowiecka, O, Taran, L., Johansson, Å., Pécskay, Z., Demaiffe, D., Grabowski, J., and Zieliński, G., 2017. Geological Map of Crystalline Basement in the Polish part of the East European Platform 1:1 000 000. Państwowy Instytut Geologiczny, Warszawa.

Krzywiec, P., Lis, P., Buffenmyer, V., Malinowski, M., and Lewandowski, M., 2013. Regional Geologic Characterization of the Polish Lower Paleozoic Unconventional Play Using an Integrated Seismic and Well Data Approach, in Unconventional Resources Technology Conference, Denver, Colorado, 12–14 August 2013, Society of Exploration Geophysicists, American Association of Petroleum Geologists, Society of Petroleum Engineers, 183–187.

Krzywiec, P., Mazur, S., Gągała, Ł., Kufrasa, M., Lewandowski, M., Malinowski, M., and Buffenmyer, V., 2017a. Late Carboniferous thin-skinned compressional deformation above the SW edge of the East European craton as revealed by seismic reflection and potential field data – Correlations with the Variscides and the Appalachians, in GSA Memoirs: Linkages and Feedbacks in Orogenic Systems. Geological Society of America, 213, 353–372.

Krzywiec, P., Gągała, Mazur, S., Słonka, Kufrasa, M., Malinowski, M., Pietsch, K., and Golonka, J., 2017b. Variscan deformation along the Teisseyre-Tornquist Zone in SE Poland: Thick-skinned structural inheritance or thin-skinned thrusting?. Tectonophysics, 718, 83–91. https://doi.org/10.1016/j.tecto.2017.06.008

Krzywiec, P., Poprawa, P., Mikołajczak, M., Mazur, S., Malinowski, M., 2018. Deeply concealed half-graben at the SW margin of the East European Craton (SE Poland) – Evidence for Neoproterozoic rifting prior to the break-up of Rodinia. J. Palaeogeogr. 7 (1), 88–97.

Kukkonen, I. T. and Lahtinen, R., 2006. Finnish reflection experiment FIRE 2001–2005. Geological Survey of Finland.

Lahtinen, R., Korja, A., Nironen, M., Heikkinen, P., 2009. Palaeoproterozoic accretionary processes in Fennoscandia, Geol. Soc. London Spec. Publ., 318, 237–256. https://doi.org/10.1144/SP318.8

Majdański, M., 2012. The structure of the crust in TESZ area by Kriging interpolation. Acta Geophysica 60(1), 59-75. https://doi.org/10.2478/s11600-011-0058-5

Malinowski, M., 2016. Deep reflection seismic imaging in SE Poland using extended correlation method applied to PolandSPAN^{TM} data. Tectonophysics, 689, 107–114. https://doi.org/10.1016/j.tecto.2016.01.007

Malinowski, M., Guterch, A., Narkiewicz, M., Probulski, J., Maksym, A., Majdański, M., Środa, P., Czuba, W., Gaczyński, E., Grad, M., Janik, T., Jankowski, L., and Adamczyk, A., 2013. Deep seismic reflection profile in Central Europe reveals complex pattern of Paleozoic and Alpine accretion at the East European Craton margin. Geophys. Res. Lett., 40, 3841–3846. https://doi.org/10.1002/grl.50746

Malinowski, M., Guterch, A., Narkiewicz, M., Petecki, Z., Janik, T., Środa, P., Maksym, A., Probulski, J., Grad, M., Czuba, W., Gaczyński, E., Majdański, M., and Jankowski, L., 2015. Geophysical constraints on the crustal structure of the East European Platform margin and its foreland based on the POLCRUST-01 deep reflection seismic profile. Tectonophysics, 653, 109–126. https://doi.org/10.1016/j.tecto.2015.03.029

Marfurt, K. J., 2018. Seismic Attributes as the Framework for Data Integration Throughout the Oilfield Life Cycle. SEG Books.

Mazur, S., Mikolajczak, M., Krzywiec, P., Malinowski, M., Buffenmyer, V., and Lewandowski, M., 2015. Is the Teisseyre-Tornquist Zone an ancient plate boundary of Baltica?. Tectonics, 34, 2465–2477. https://doi.org/10.1002/2015TC003934

Mazur, S., Mikolajczak, M., Krzywiec, P., Malinowski, M., Lewandowski, M., and Buffenmyer, V., 2016a. Pomeranian Caledonides, NW Poland – A collisional suture or thin-skinned fold-and-thrust belt?. Tectonophysics, 692, 29–43. https://doi.org/10.1016/j.tecto.2016.06.017

Mazur, S., Mikolajczak, M., Krzywiec, P., Malinowski, M., Buffenmyer, V., and Lewandowski, M., 2016b. Reply to Comment by M. Narkiewicz and Z. Petecki on “Is the Teisseyre-Tornquist Zone an ancient plate boundary of Baltica?”. Tectonics, 35, 1600–1607. https://doi.org/10.1002/2016TC004162

Mazur, S., Aleksandrowski, P., Gągała, Ł., Krzywiec, P., Żaba, J., Gaidzik, K. and Sikora, R., 2020. Late Palaeozoic strike-slip tectonics versus oroclinal bending at the SW outskirts of Baltica: case of the Variscan belt’s eastern end in Poland. International Journal of Earth Sciences, 109, 1133–1160, https://doi.org/10.1007/s00531-019-01814-7.

Mężyk, M., Malinowski, M., Mazur, S., 2019. Imaging the East European Craton margin in northern Poland using extended correlation processing of regional seismic reflection profiles. Solid Earth, 10, 683–696.

Mężyk, M., and Malinowski, M., 2019. Multi-pattern algorithm for first-break picking employing open-source machine learning libraries. Journal of Applied Geophysics, 170.

Mężyk, M., and Malinowski, M., 2020. Deep embedded clustering as a seismic attribute: a case study of 2D crustal-scale interpretation, in 82th EAGE Conference and Exhibition, Amsterdam.

Mikołajczak M., Mazur S., Gągała Ł., 2019. Depth-to-basement for the East European Craton and Teisseyre-Tornquist Zone in Poland based on potential field data. Int J Earth Sci, 108(2), 547–567. https://doi.org/10.1007/s0053 1-018-1668-9

Milano, M., Fedi, M., Fairhead, J. D., 2019. Joint analysis of the magnetic field and total gradient intensity in central Europe. Solid Earth, 10, 697-712.

Młynarski S., 1982. The structure of deep basement in Poland in the light of refraction seismic surveys. Geological Quarterly, 26(2), 285–296.

Narkiewicz M., Grad M., Guterch A., Janik T., 2011. Crustal seismic velocity structure of southern Poland: preserved memory of a pre-Devonian terrane accretion at the East European Platform margin. Geological Magazine, 148, 191–210.

Okaya, D. A., and Jarchow, C. M., 1989. Extraction of deep crustal reflections from shallow Vibroseis data using extended correlation. Geophysics, 54, 555–562. https://doi.org/10.1190/1.1442682

Pacześna, J., 2014. Lithostratigraphy of the Ediacaran deposits in the Lublin-Podlasie sedimentary basin (eastern and south-eastern Poland). Biuletyn Państwowego Instytutu Geologicznego, 460, 1–24.

Pedregosa, F., Varoquaux, G., Gramfort, A., Michel, V., Thirion, B., Grisel, O., Blondel, M., Prettenhofer, P. Weiss, R., Dubourg, V., Vanderplas, J., Passos, A., Cournapeau, D., Brucher, M., Perrot, M., Duchesnay, E., 2011. Scikit-learn: Machine Learning in Python. Journal of Machine Learning Research, 12, 2825-2830.

Petecki Z., and Rosowiecka O., 2017. A new magnetic anomaly map of Poland and its contribution to the recognition of crystal line basement rocks. Geological Quarterly, 61, 934-945.

Poprawa, P., and Pacześna, J., 2002. Late Neoproterozoic to Early Palaeozoic development of a rift at the Lublin–Podlasie slope of the East European Craton–analysis of subsidence and facies record (eastern Poland). Przegląd Geologiczny, 50, 49–63 [in Polish with English summary].

Poprawa, P., Krzemińska, E., Pacześna, J. and Amstrong, R., 2020. Geochronology of the Volyn volcanic complex at the western slope of the East European Craton–relevance to the Neoproterozoic rifting and the break-up of Rodinia/Pannotia. Precambrian Research, 346, 105817. https://doi.org/10.1016/j.precamres.2020.105817

Shcherbak, N.P., Artemenko, G.V., Skobelev, V.M., Stepanyuk, L.M., Ponomarenko, O.M., 2002. Geochronology of the Precambrian of the Ukrainian Shield on the basis of the "Reference" isotope data. Miner. J., 24: 87–110.

Shumlyanskyy, L., Billström, K., Hawkesworth, C., Elming, S.-Å., 2012. U-Pb age and Hf isotope compositions of zircons from the north-western region of the Ukrainian shield: mantle melting in response to post-collision extension. Terra Nova, 24, 373–379.

Skridlaite, G., and Motuza, G., 2001. Precambrian domains in Lithuania: evidence of terrane tectonics. Tectonophysics, 339, 113–133.

Taran, L.N., and Bogdanova, S.V., 2001. The Fennoscandia–Sarmatia junction in Belarus: new inferences from a PT-study. Tectonophysics, 339, 193–214.

Taran, L.N., and Bogdanova, S.V., 2003. Metamorphism of the Palaeoproterozoic paragneisses of the Belarus–Podlasie Granulite Belt: a prograde–retrograde evolution. Petrology (Petrologija), 11, 444–461.

Torvela, T., Moreau, J., Butler, R. W. H., Korja, A., Heikkinen, P., 2013. The mode of deformation in the orogenic mid-crust revealed by seismic attribute analysis. Geochemistry, Geophysics, Geosystems, 14, 1069– 1086.

Trofimov, V. A., 2006. Deep CMP seismic surveying along the Tatseis-2003 geotraverse across the Volga-Ural petroliferous province. Geotectonics, 40(4), 249–262.

West, B. P., May, S. R., Eastwood, J. E., Rossen, C., 2002. Interactive seismic facies classification using textural attributes and neural networks. The Leading Edge, 21(10), 1042–1049.

White, D.J., Thomas, M.D., Jones, A.G., Hope, J., Németh, B., Hajnal, Z., 2005. Geophysical transect across a Paleoproterozoic continent–continent collision zone: The Trans- Hudson Orogen. Canadian Journal of Earth Sciences, 42(4): 385-402.